Title
InSAR and GPS measurements of crustal deformation due to seasonal loading of Tehri reservoir in Garhwal Himalaya, India

Journal
Geophysical Journal International, 209(1)

ISSN
0956-540X

Authors
Gahalaut, VK
Yadav, Rajeev K
Sreejith, KM
et al.

Publication Date
2017

DOI
10.1093/gji/ggx015

Peer reviewed

InSAR and GPS measurements of crustal deformation due to seasonal loading of Tehri reservoir in Garhwal Himalaya, India

V.K. Gahalaut,[1] Rajeev K. Yadav,[2] K.M. Sreejith,[3] Kalpna Gahalaut,[2] Roland Burgmann,[4] Ritesh Agrawal,[3] S.P. Sati[5] and Amit Bansal[2]

[1]National Centre for Seismology, Ministry of Earth Sciences, New Delhi 110003, India. E-mail: vkgahalaut@yahoo.com [2]CSIR-National Geophysical Research Institute, Hyderabad, Telangana 500007, India [3]ISRO-Space Applications Center, Ahmedabad, Gujarat 380015, India [4]Department of Earth and Planetary Science, University of California, Berkeley, CA 94709, USA [5]Department of Geology, HN Bahuguna Garhwal University, Srinagar, Uttarakhand 246174, India

Summary

We report unique observations of crustal deformation caused by the seasonal water level changes of Tehri reservoir in the Garhwal region of NW Himalaya from GPS measurements and Interferometric Synthetic Aperture Radar (InSAR) analysis. All GPS sites along the Himalaya are strongly influenced by seasonal hydrological and atmospheric loading. However, the GPS site KUNR located near the reservoir additionally exhibits anomalous variations due to seasonal water loading and unloading by the reservoir. Our InSAR analysis confirms that the seasonal filling of the reservoir causes measurable subsidence in its neighbourhood. In addition to the elastic deformation caused by the seasonal reservoir loading and the negligible poroelastic deformation caused by associated fluid pressure changes, there is an unaccounted biannual deformation in the east component of the GPS time-series which we suspect to be caused by altered hydrological conditions due to the reservoir operations. Understanding crustal deformation processes due to such anthropogenic sources helps in separating deformation caused by tectonic, hydrological and atmospheric effects from that caused by these activities.

Key words: Loading of the Earth; Space geodetic surveys; Asia

INTRODUCTION

Human activities, such as mining, fluid injection and extraction, reservoir impoundment, waste disposal, etc. may alter physical conditions (Simpson 1986) thereby changing the stress state and hydrological conditions in the surrounding medium. Reservoir impoundments for hydroelectricity generation, due to their large size and associated water load, may cause measurable deformation and are considered to have triggered strong earthquakes. Although there are several cases where impoundment of reservoirs has been considered to have triggered earthquakes (Gupta 1992), by deforming the underlying material and thereby modifying the ambient stresses, the link between the two has always been conjectural. There have been several direct measurements of the influence of reservoir impoundment in terms of deformation and pore pressure. Kaufmann & Amelung (2000) reported the subsidence caused by the impoundment of

Lake Mead reservoir, based on levelling observations which were undertaken in 1935 before completion of dam construction and then after the impoundment in 1941, 1950 and 1963. This was further taken up by Cavalié *et al*. (2007) who used Interferometric Synthetic Aperture Radar (InSAR) to quantify the deformation during 1992–2002 at Lake Mead reservoir, used the same viscoelastic model as Kaufmann & Amelung (2000), and confirmed that viscoelastic relaxation contributed to the time-dependent deformation caused by the reservoir impoundment. Wang (2000a) predicted the land level changes due to impoundment of the ~600-km long Three Gorges reservoir. Wang *et al*. (2011) used InSAR to analyse the dam deformation caused by the Three Gorges reservoir impoundment. Wahr *et al*. (2013) analysed GPS measurements at sites close to Lake Shasta in California to confirm the 2007–2010 drought related deformation.

Here, we report on crustal deformation caused by loading and unloading of Tehri reservoir through InSAR analysis and continuous measurement at a permanent GPS site. A permanent GPS network of 23 sites in the Garhwal Kumaun Himalaya has been installed for monitoring crustal deformation and understanding strain accumulation in the Himalayan region. One of the GPS sites, KUNR (Fig. 1) is located close to the reservoir created by the 260.5 m high Tehri Dam, which started operating in 2006. The dam is located on the confluence of the Bhagirathi and Bhilangana rivers, which are tributaries to the river Ganga (or the Ganges). The predominant rock type in the region is phyllite, belonging to the Lesser Himalayan sequence. The reservoir has a total volume of ~4 km^3 at full capacity with a surface area of ~52 km^2 and water depths reaching of up to ~214 m at the dam during lake level highstands (Figs 1c and d). The reservoir is impounded largely on the Bhagirathi river and extends up to a distance of ~30 km to the northwest from the dam. We employ InSAR analysis to estimate the spatial pattern of the deformation caused by the seasonal changes of the reservoir level. Continuous GPS measurements at KUNR and other sites of our GPS network help in understanding the complexities in temporal variations in the deformation caused by the Tehri reservoir operations and separating contributions to seasonal deformation from regional hydrological loading (e.g. Bettinelli *et al*. 2008). Models of elastic loading and poroelastic deformation are compared with the observed spatial and temporal patterns of deformation obtained from the InSAR analysis and GPS measurements.

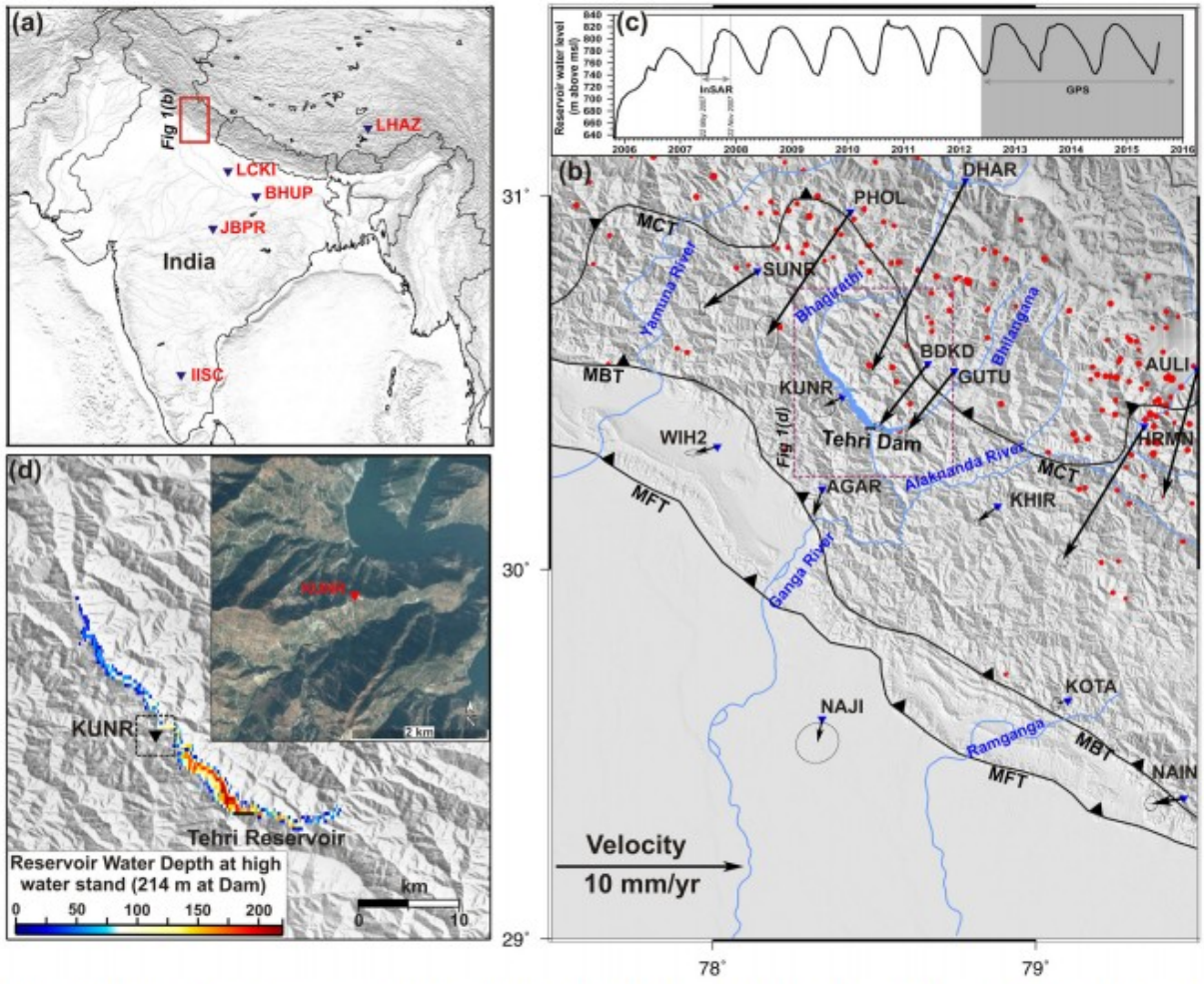

Figure 1. (a) Location of GPS measurement sites using here. (b) Part of the GPS network in the Garhwal-Kumaun Himalaya. Site motion is shown in the Indian reference frame. Red filled circles are the earthquakes of $M \geq 4$ during 1964–2015 from ISC and EHB catalogues. White contour marks the 3500 m topography. (c) Tehri reservoir water variations at the dam site (cwc.gov.in). Periods of InSAR analysis and GPS measurements are indicated by labelled double arrows. (d) Considered reservoir water depths at highwater stand. 0 corresponds to 620 m, the height of the base of the reservoir from mean sea level. Inset in this panel show a zoomed image (from Google Earth) of the region around KUNR.

INSAR ANALYSIS OF DEFORMATION DUE TO TEHRI RESERVOIR AND ITS SIMULATION

Before we analyse the seasonal variations in GPS measurements at KUNR and other sites, we describe our InSAR analysis of the spatial pattern of deformation caused by the Tehri reservoir in its neighbouring region. After the impoundment, SAR data were acquired by PALSAR sensor of the ALOS-1 satellite during 2007–2008 (on dates as 2007 February 19, 2007 May 22, 2007 August 22, 2007 November 22, 2008 January 7 and 2008 July 9). Interferograms were generated using GMTSAR software (Sandwell *et al*. 2011) and unwrapped using SNAPHU software (Chen & Zebker 2001). The interferometric phase changes corresponding to topography were removed using Shuttle Radar Topographic Mission (SRTM) data of 30 m spatial resolution. A best-fit quadratic plane is subtracted from the interferograms to reduce effects of orbital and ionospheric perturbations. We generated a total

of nine interferograms with the idea of employing a small baseline subset strategy to generate time-series of deformation with respect to the scene acquired on 2007 May 22, which corresponds to a low water stand in the reservoir. However, interferograms formed using scenes acquired on 2007 August 22 and 2008 July 9 showed significant atmospheric signals and hence were avoided in the analysis. We have selected the three interferograms with maximum correlation and minimum atmosphere-related signals and stacked them together to generate the deformation map between 2007 May 22 and November 22. Thus, the deformation map represents the surface displacements between the lowest and highest water levels during this period. The deformation map shows significant line of sight (LOS) displacements (Fig. 2a) that increase towards the reservoir. To analyse the spatial pattern of LOS and to verify that the LOS close to the reservoir is due to reservoir filling, we simulate the displacement due to change in reservoir water level during 2007 May 22 and November 22.

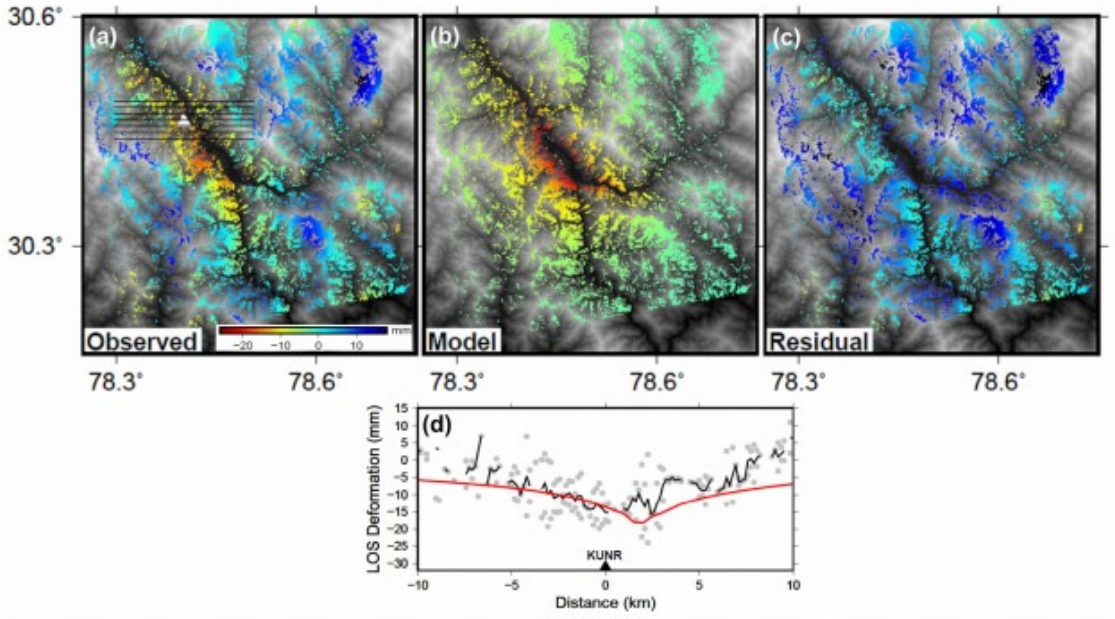

Figure 2. (a) Observed LOS deformation from InSAR due to difference in water levels in the Tehri reservoir on 22 May 2007 and 22 November 2007, (b) simulated LOS deformation from Fig. 3, and (c) the residual between the observed and simulated LOS deformation. (d) West-east profile passing through the KUNR GPS site. Black broken lines and grey dots are the median and scatter in the LOS deformation along a 1-km-wide swath across the InSAR image. Corresponding simulated displacement due to the reservoir is also shown by red line.

We discretize the reservoir water load into 629 rectangles and water level is assigned to each of these rectangles according to its bathymetry in Google Earth. The computed total water capacity of the simulated reservoir is consistent with the actual water capacity of the reservoir (4 km^3) with maximum water level of ~214 m at the dam site (Fig. 1d). Water level in each of these rectangular cuboids is varied, which is constrained by the seasonal water elevation history at the dam site. We use Boussinesq solutions (Jaeger *et al*. 2007) for calculating elastic deformation around the reservoir due to the seasonal loading and unloading of an elastic half-space. We assumed a Poisson's solid ($\nu = 0.25$) and considered a range of shear

modulus values from 28 to 36 GPa. We used a value of 32 GPa as it better fits the observations. We also considered the displacement caused by pore pressure diffusion. We calculated pore pressure by solving the diffusion equation and then computed the corresponding displacement components (Jónsson *et al*. 2003 and Wang 2000b). However, its contribution turned out to be insignificant, reaching a maximum value of <~0.1 mm in the vertical and 0.05 in the horizontal close to the reservoir, which decays with distance. From here onwards, we only consider the elastic deformation due to surface loads. The computed total displacement field in the region around the reservoir caused by the difference in reservoir load between low (741 m above msl or 121 m water depth at dam) and high water stands (811 m above msl or 191 m water depth at dam), on 2007 May 22 and November 22, respectively, is shown in Fig. 3. This corresponds to a reservoir water level difference of 70 m at the dam which decreases in the upstream side in the reservoir. The simulated displacement field shows large subsidence and relatively insignificant horizontal displacements. In general, reservoir loading causes more displacement in the vertical direction compared to that in the horizontal direction (Gahalaut & Kalpna 2001). The ratio between vertical to horizontal displacement is more than three (Wahr *et al*. 2013) at a distance of more than 10 km from the reservoir and is much larger in the region within 10 km of the reservoir, implying that the vertical deformation dominates in reservoir loading.

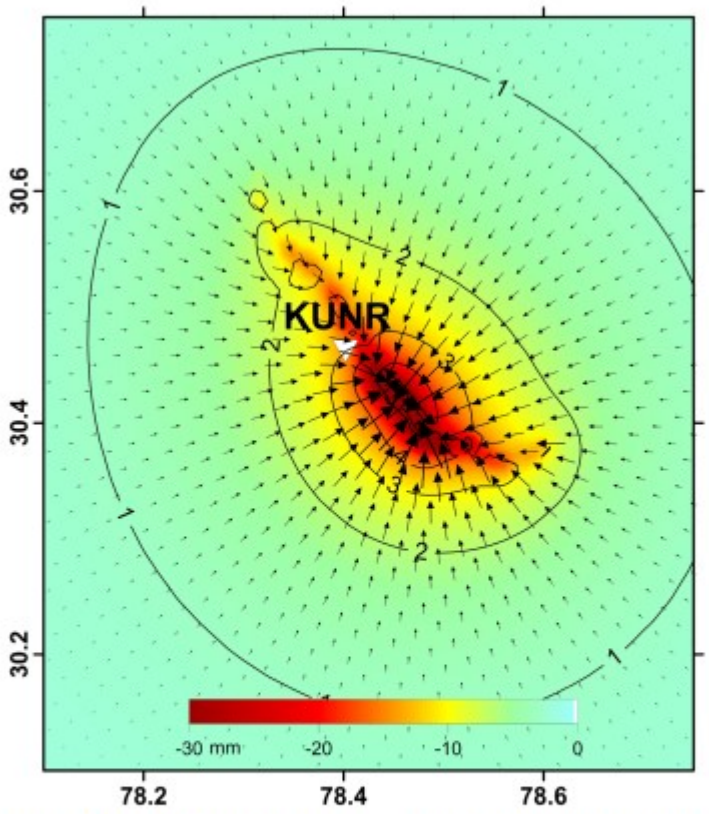

Figure 3. Simulated horizontal and vertical elastic deformation due to difference in water levels in the Tehri reservoir on 22 May 2007 (191 water depth at dam) and 22 November 2007 (121 m water depth at dam) and its negligible poroelastic relaxation. Contours and arrows show the horizontal displacement while the colour image shows the vertical displacement. All units in mm. KUNR GPS site also shown.

We projected the simulated displacement of Fig. 3 into the LOS and find good agreement with that obtained from the InSAR analysis (Fig. 2a) with a shear modulus of 32 GPa. The remaining residual signal (Fig. 2c) appears to be topography correlated and is likely due to atmospheric delay. Fig. 2(d) also shows change in LOS along an east–west profile passing through the KUNR GPS site.

GPS MEASUREMENTS IN THE GARHWAL KUMAUN HIMALAYA

In 2012–2013, a network of 23 GPS sites was installed in the Garhwal Kumaun region to monitor the crustal deformation and strain accumulation along this part of the Himalayan arc. These sites span all the geological units of the Himalayan arc and the adjoining Indo-Gangetic plains. Continuous GPS data from these stations, along with other sites in the Indian region (Fig. 1), have been analysed together with several IGS sites surrounding the Indian plate. We used GAMIT, version 10.60 (King & Bock 2005; Herring *et al*. 2010a,b), to estimate the time-series of site coordinates and their mean velocities. Site position estimates and their rates were estimated in ITRF2008 (Altamimi *et al*. 2011) by stabilizing sites in stable continental regions and

core IGS reference sites using GAMIT/GLOBK, GLORG. We have used the GMF (Global Mapping Function) and a priori pressure and temperature from the GPT2 model have been used in absence of in situ meteorological data (Boehm *et al*. 2006a; Lagler *et al*. 2013). The ocean tide model FES2004 (Letellier 2004) has been used for the removal of contributions from ocean tidal loads at the site locations. The IERS2003 model has been used for the correction of site displacement associated with solid earth deformation produced by tidal potential (McCarthy & Petit 2004).

These sites show northeastward motion varying from 50 to 36 mm yr^{-1} in ITRF2008. In the Indian reference frame these sites show arc-normal, predominantly southward motion (Fig. 1b). Sites in the Indo-Gangetic plains show almost no motion while the southward motion progressively increases at sites located in the north and reaches a maximum of about ~14 mm yr^{-1} in the Higher Himalaya. This secular motion is consistent with the strain accumulation on the underlying Main Himalayan Thrust, MHT (e.g. Ader *et al*. 2012). One of the sites of the network, KUNR, is located very close to the reservoir created by the Tehri Dam (Fig. 1d). It is ~12 km northwest of the dam in the upstream direction, and is less than 1 km from the right bank of the reservoir on the Bhagirathi river. We analyse seasonal variations in displacement time-series at this and other GPS sites.

SEASONAL VARIATIONS IN THE GPS TIME-SERIES DUE TO ATMOSPHERIC AND HYDROLOGICAL LOADS

Apart from the secular motion which varies according to the distance from the Himalayan front and occurs in response to the India-Eurasia convergence and strain accumulation on the MHT, all the sites in the Himalayan and adjoining regions show strong seasonal variations. We remove the average velocities from all the time-series and analyse the seasonal variations only. Seasonal variations have been previously reported in the Himalayan region (Bollinger *et al*. 2007; Bettinelli *et al*. 2008; Flouzat *et al*. 2009; Fu & Freymueller 2012; Chanard *et al*. 2014; Khandelwal *et al*. 2014). Bettinelli *et al*. (2008) proposed that these seasonal variations are due to the recharging/ loading of the Indo-Gangetic Plain due to precipitation. In addition, atmospheric pressure change (van Dam & Wahr 1987; van Dam 2010; Chanard *et al*. 2014) and accumulation and melt of snow and ice in the Himalaya (Fu & Freymueller 2012) can also contribute to the seasonal variations in the GPS time-series. Chanard *et al*. (2014) analysed GPS data from the Nepal Himalaya and considered contributions from atmospheric, hydrological and non-tidal oceanic loads. They used a spherical layered earth model and concluded that the observed seasonal variations are in phase with the simulated variations. Seasonal variations in the Himalayan region are most prominent in the vertical and north components of GPS time-series.

We estimate seasonal variations in the three displacement components due to corresponding seasonal variations in the atmospheric and hydrological loads using global models and compare them with the GPS time-series at all

sites. Farrell (1972) provided Green's functions which describe the response of an elastic earth to a point load on its surface. The radial and horizontal displacements at any point on the surface of the earth can be estimated by evaluating a convolution between the Green's functions and load functions. Horizontal changes in the atmospheric mass are governed by pressure loading at the surface and the gravitational attraction of the atmospheric mass. These variations in the horizontal distribution of atmospheric mass induce deformation within the earth (van Dam & Wahr 1987). We used the data and programs provided by the Global Geophysical Fluid Center (GGFC; van Dam & Wahr 1987; van Dam 2010, http://geophy.uni.lu/ggfc-atmosphere/ncep-loading.html) for the estimation of surface displacements at the GPS sites due to the atmospheric pressure loading. GGFC provides 6-hourly, global surface displacements at 2.5°×2.5° resolution, derived from National Center for Environmental Protection's (NCEP) reanalysis of surface pressure. For the estimation of surface displacement due to hydrological load, we used the data and program provided by GFZ (ftp://ig2-dmz.gfz-potsdam.de/LOADING/HYDL). The hydrological load is taken from the hydrological Land Surface Discharge Model (LSDM) which includes daily estimates of soil moisture, snow, and surface water mass in rivers and lakes on a regular grid 0.5°×0.5° (Dill 2008; Dill 2013). Hydrologically induced elastic surface deformation is calculated by convolving Farrell's Green's function with modelled hydrological mass distributions from the LSDM. The elastic deformation has been computed in the centre of Earth's figure frame (cF) on the basis of load Love numbers given for the elastic Earth model ‘ak135' (Wang *et al*. 2012).

To visualise the spatial variation of the atmospheric and hydrological loads and their effect on the deformation, we show the variations in load-derived displacement and seasonal variations in the GPS time-series at a few sites, located in southern China (LHAZ in Fig. 4), the Indo-Gangetic Plain (LCKI, BHUP, JBPR in Fig. 5) and southern India (IISC in Fig. 6), along with sites in the Himalaya (Fig. 7). Strong spatial variations in the seasonal load and associated predicted vertical displacement can be seen from north to south. The winter loads are smallest in southern China (LHAZ) and southern India (IISC). Snowfall in the winter contributes to subsidence in the Higher Himalaya, whereas the precipitation and runoff from the mountains during the same period contributes to the load in the Indo-Gangetic Plain (Figs 4–7). The variations in displacement due to hydrological loading dominate over atmospheric loading. For example, at a site GUTU, the variations due to hydrological load are ±3, ±1.7, ±8.5 mm in the north, east and vertical components while that due to atmospheric load are ±1, ±1, ±6 mm in the north, east and vertical components. At all sites the vertical component of GPS measurements is consistent with that derived from the atmospheric and hydrological loads. Although there is a general consistency between the horizontal components of GPS measurements and that derived from the atmospheric and hydrological loads, at some sites there are differences in

the phase between the two (e.g. the north component at DHAR, Fig. 7, and LCKI, Fig. 5b, and east component at GUTU, Fig. 7). Fu *et al*., (2013) also noted similar phase differences at some sites in the Nepal Himalaya. Amongst all the time-series analysed here, the east component displacement at KUNR is anomalous and is inconsistent with that derived from the loads.

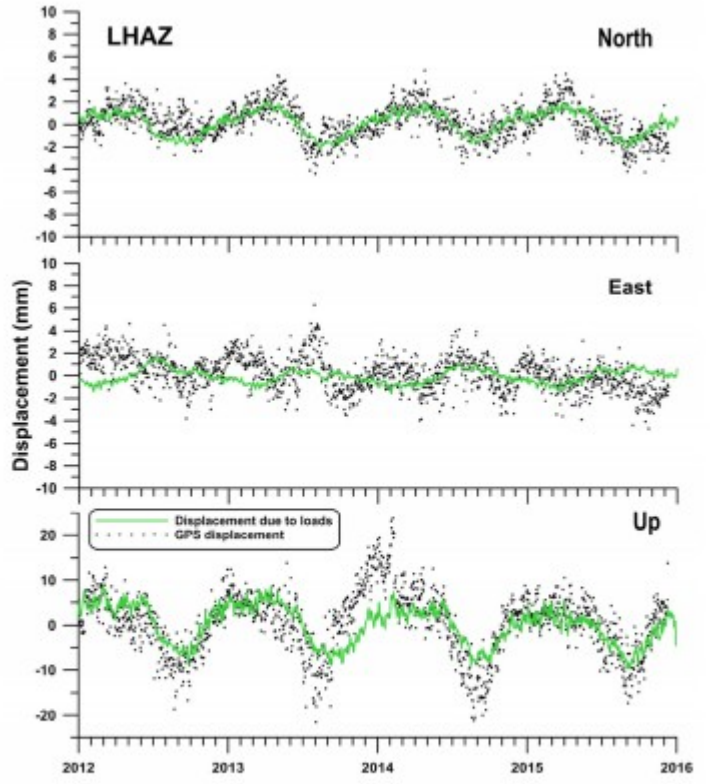

Figure 4. Seasonal variations in the north, east and up components of GPS time-series at LHAZ (black dots). Green curve in each panel is the displacement simulated from the atmospheric and hydrological loads.

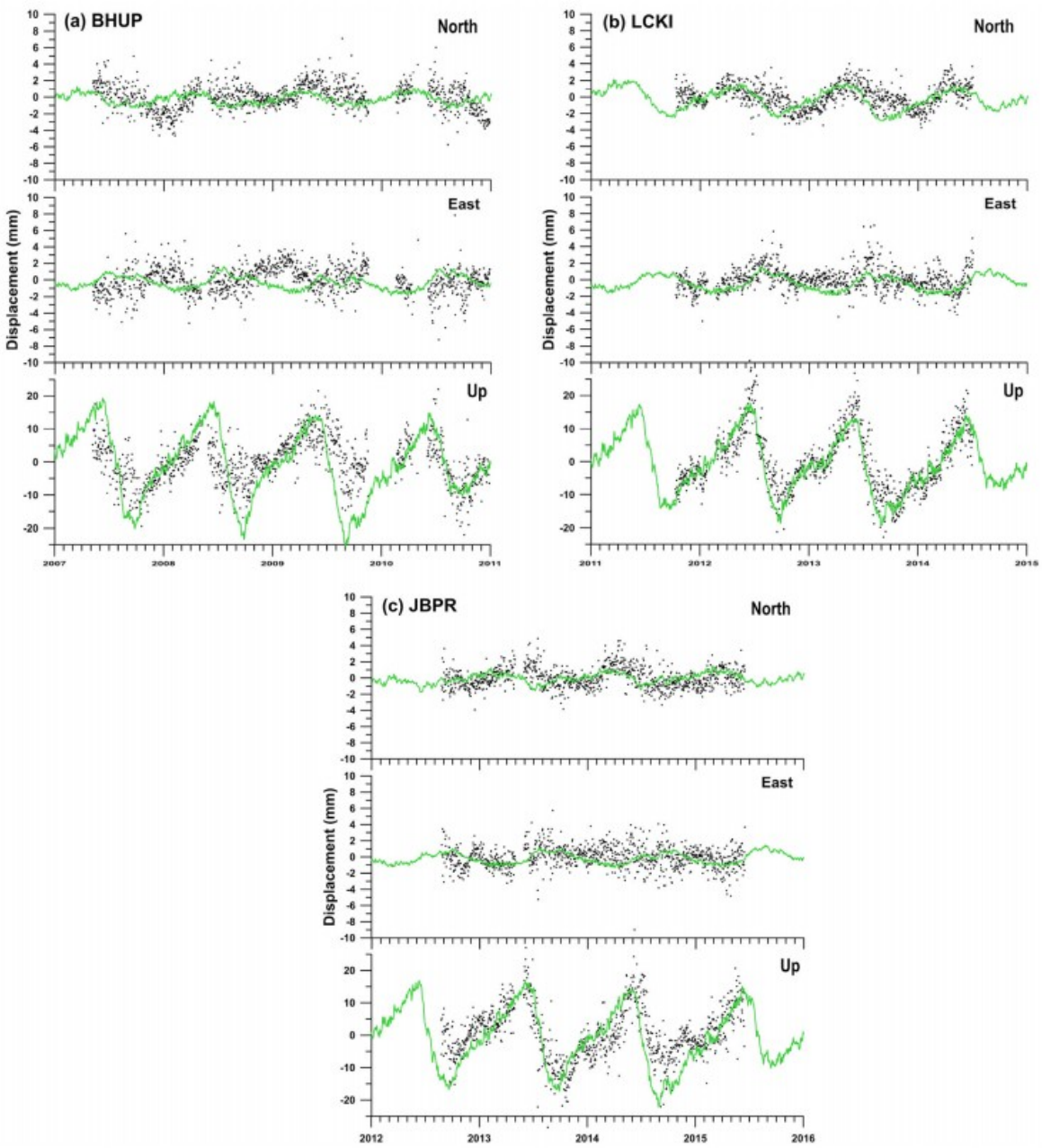

Figure 5. Same as Fig. 4 but for sites BHUP, LCKI and JBPR in the Indo-Gangetic plains.

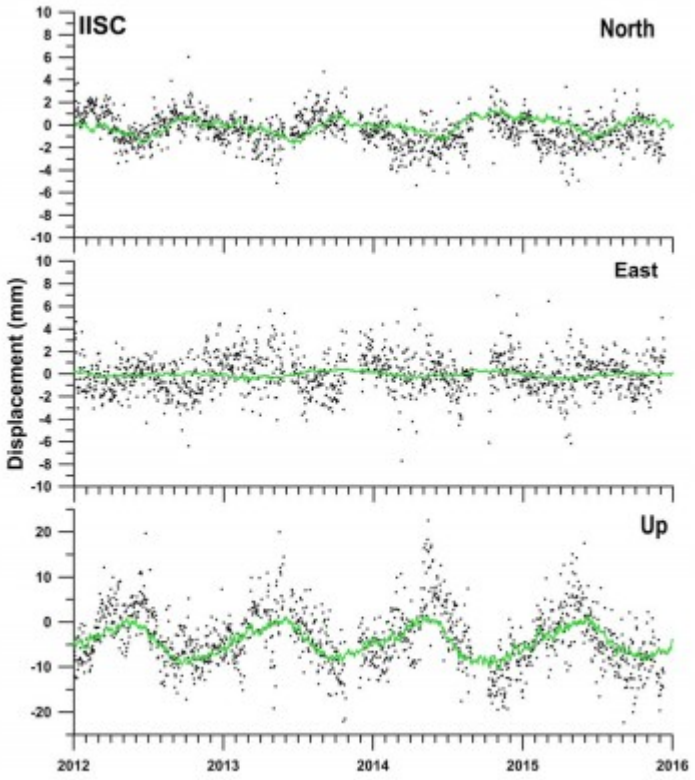

Figure 6. Same as Fig. 4 but at site IISC in south India.

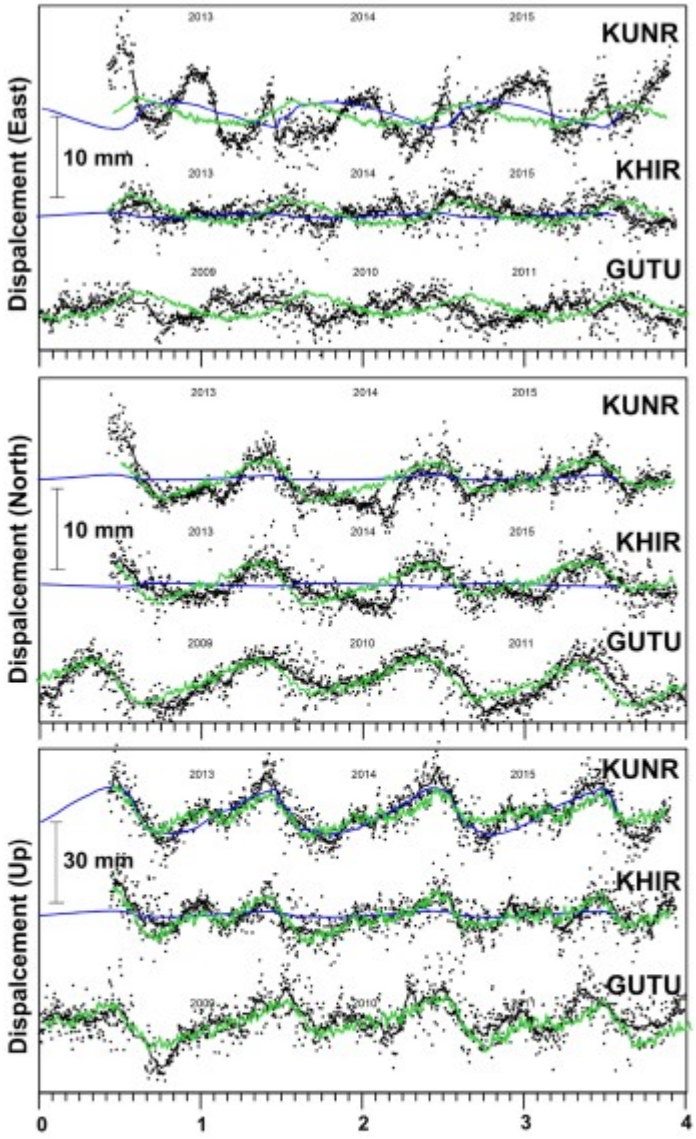

Figure 7. Comparison of east, north and up components of seasonal variations at GPS time-series at KUNR, KHIR and GUTU. The continuous curve in each component is the running average using a 21-day window. Green curve in each panel is the displacement simulated from the atmospheric and hydrological loads. Blue curves at KHIR and KUNR is the simulated elastic displacement due to the Tehri reservoir loading and unloading. Note the anomalous behaviour in the east component at KUNR. Also note that the period of observations of GPS measurements at GUTU is different and change in scale in the Up component.

ANOMALOUS TEMPORAL VARIATION IN DISPLACEMENT AT GPS SITE KUNR

The motion at site KUNR, located <1 km from the reservoir, is anomalous in many aspects. We compare the motion at this site with the nearby sites at KHIR and GUTU (Fig. 7) which are 56 and 34 km to the southeast and east-northeast from KUNR, respectively. Seasonal variations in the north are quite similar at the three sites but those in the east and up components at KUNR

are large in comparison to those observed at GUTU and KHIR. We used data from GUTU due to availability of continuous data from this site, though the period of data is different. Another site, BDKD, which has data from the same period as KUNR and KHIR, and is close to GUTU, show similar behaviour but has data gaps. We hypothesise that the large variations in the east and up components are because of the proximity of KUNR site to the Tehri reservoir.

The temporal variation in elastic displacement due to reservoir loading at site KUNR is estimated by the same method as discussed above. Simulated displacement in Fig. 7 indicates that seasonal filling of the reservoir during the monsoon causes subsidence and eastward movement at KUNR, as also seen in Fig. 3. Because of the orientation of the reservoir and the location of KUNR (Fig. 3), variations in the north component of simulated displacements are insignificant (Fig. 7). The good fit of the simulated displacement due to the reservoir to the InSAR data implies that the simulated displacement due to reservoir operations is generally correct. Thus we subtract the influence of atmospheric and hydrological loads KUNR GPS time-series. This would, in principle, reflect the influence of reservoir. We compare this (red curve in Fig. 8) with the derived displacement due to reservoir response (blue curve in Fig. 8). The two are approximately consistent in the north and up components but there is significant variations between the two in east component with residual KUNR time-series showing biannual variations of amplitude ±4 mm, while that caused by the reservoir load is annual and is less than ±2 mm. Thus the observed variation of displacement in the east component is not consistent with that predicted by the reservoir operation.

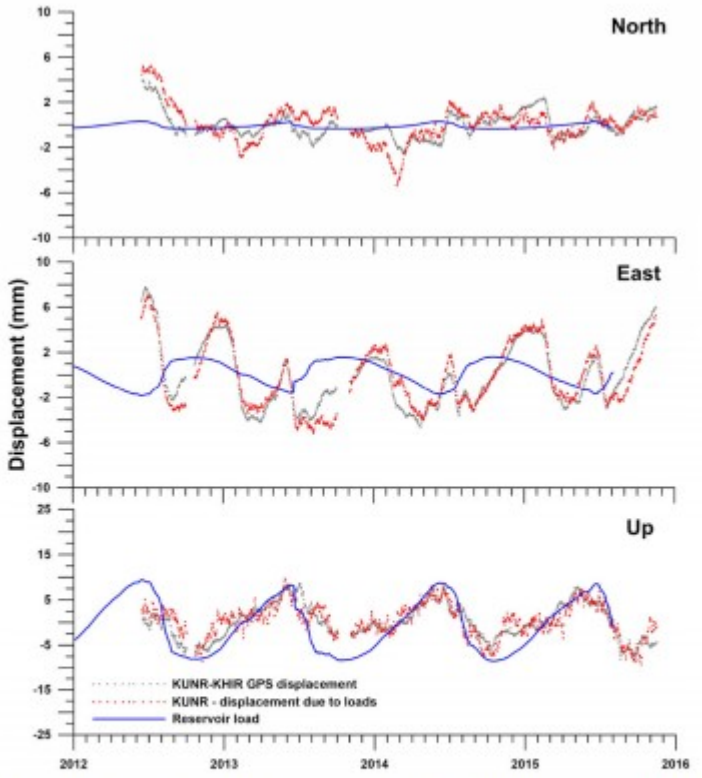

Figure 8. Comparison of the reservoir induced elastic displacement (blue curve) with the residual displacement obtained after subtracting the contributions of hydrological and atmospheric loads from the KUNR GPS time-series (red dotted curve) and also with the subtraction of displacement time-series of KHIR from KUNR (grey dotted curve).

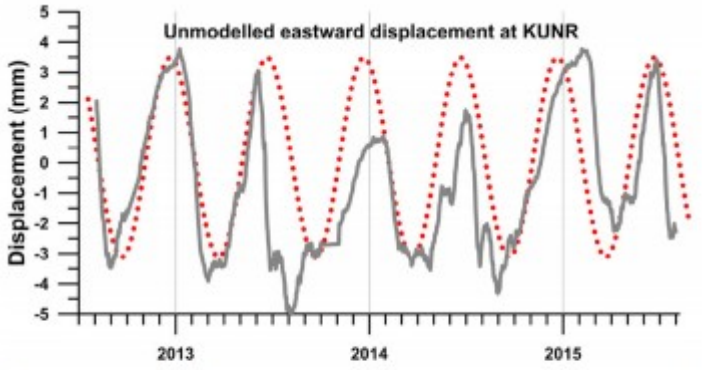

Figure 9. Net residual displacement in east component at KUNR, after subtracting the GPS displacement time-series of KHIR and reservoir induced elastic displacement at KUNR from KUNR GPS time-series. Red dotted curve is a biannual sinusoidal curve approximating the net residual.

DISCUSSION

The observed spatial pattern of deformation near Tehri dam in our InSAR analysis is consistent with the simulated pattern of deformation due to the local reservoir load. The LOS displacements in the InSAR measurement are

dominated by the vertical component. The modelled horizontal deformation, particularly near the reservoir is small, in comparison with the vertical deformation. The change in the vertical in the KUNR GPS time-series between high and low water stand is also consistent with the simulated reservoir displacement and regional hydrological and atmospheric loading. The GPS time-series of the vertical and north components from stations analysed here, other than KUNR, are generally well matched by a regional model of seasonal hydrological/atmospheric loading, consistent with similar results in Nepal (Bettinelli *et al*. 2008; Fu & Freymueller 2012; Chanard *et al*. 2014). The observed biannual variation in the eastward displacement of the KUNR GPS time-series is clearly anomalous. The magnitude of this variation is too small to be picked up in the InSAR analysis. Further, as the InSAR images could be generated only at low and high water stands, there is no way we could verify the biannual behaviour of the eastward displacement.

Considering that displacement components derived from the atmospheric and hydrological loads are not very detailed and are not always consistent with the GPS displacement time-series, particularly in phase, we subtracted the GPS displacement time-series of the nearby site KHIR, which is located at a similar distance from the Main Frontal Thrust and Indo-Gangetic Plain, from the KUNR GPS displacement time-series. As the two sites are only 56 km apart, the atmospheric and hydrological load contributions at both sites are similar. The displacement due to the elastic loading from the reservoir and its poroelastic relaxation at KHIR is negligible (blue curve in Fig. 7). We compared the KUNR-KHIR time-series (grey curve in Fig. 8) with the reservoir load simulated displacement (blue curve in Fig. 8). Again the north and up components match well, while there is a substantial difference between the two in the east component. Even though the periods of GPS measurements and InSAR analysis are different, considering that the pattern and magnitude of annual loading and unloading of reservoir is similar (Fig. 1c), the subsidence estimated in the InSAR analysis (~17 mm) due to reservoir loading is consistent with that in the up component of the KUNR-KHIR GPS time-series (~15 mm) and also with the modelled reservoir load displacement (~15 mm). The reservoir simulated eastward displacement time-series shows annual variations, but the east component of the KUNR-KHIR GPS time-series exhibits biannual variations (Fig. 8). There appears to be an additional peak in the dry season when the reservoir water level is at its minimum. As this pattern is consistent for 3 yr, it cannot be an artefact of GPS data processing or an error in GPS measurements.

To further probe the behaviour of KUNR, we subtracted the simulated displacement in the east component due to the reservoir from the east component of the KUNR-KHIR time-series. The net residual deformation at KUNR depicts biannual variation with amplitude of ~3 mm (Fig. 9). Considering the possibility of uncertainty in the reservoir load, we uniformly changed the amplitude of reservoir simulated east component of displacement by up to ±20% but the pattern of residual displacement in Fig.

9 does not change in any significant manner. We find some difference in magnitude between the vertical component of reservoir simulated and KUNR-KHIR displacement time-series (Fig. 8), but it is within the uncertainty of GPS measurements. Thus it is only the east component of the KUNR GPS time-series which has some unexplained variations, i.e., biannual variations of ±3 mm, probably linked with the reservoir operation. Since at other neighbouring sites, which are located far away from the reservoir, such variations are not seen, we suggest that they are unlikely to be due to periodic tectonic processes. Lacking a physical explanation of the biannual changes in the east component at KUNR, we speculate that local hydrological, thermoelastic or anthropogenic processes may be at work. Further, since anomalous variations of the east component at KUNR could not be explained by the poroelastic response to the reservoir load alone, we suggest that the reservoir operations alter the geohydrological conditions in its neighbouring region (Magilligan & Nislow 2005; Cavalié *et al*. 2007), which are not captured by our simple model. However, at this stage, we are unable to explain the mechanism responsible for such variations.

CONCLUSIONS

Impoundment of large reservoirs for hydroelectric power generation can change local hydrological conditions, produce measureable crustal deformation in its surrounding and may sometimes trigger earthquakes. However, direct measurements of these effects are still limited. Through InSAR analysis and continuous GPS measurements, we provide evidence of deformation due to the filling cycles of the reservoir of the 260.5 m high Tehri Dam in the Garhwal Himalaya. Analysis of InSAR data confirms that the reservoir filling causes large subsidence in its vicinity which is consistent with the predicted poroelastic response to the annual filling of the reservoir. Time-series of continuously operating GPS stations in the surrounding Garhwal Kumaun Himalaya show a strong annual modulation in the vertical and north components that is well explained by a model of large-scale seasonal hydrological and atmospheric loading. The vertical component of a single GPS site that is located immediately adjacent to the reservoir clearly documents the combined effect of the local reservoir water load and the regional hydrological and atmospheric loading. This station also records an anomalous displacement in the east component with a biannual periodicity, which is probably linked to changes in subsurface hydrological conditions due to cyclic loading and unloading of the reservoir that are not captured by currently available models.

Acknowledgments

The GPS measurements in Garhwal Kumaun Himalaya are financially supported by Ministry of Earth Sciences (MoES/P.O.(Seismo)/1(116)/2010). Discussions with Vinod Gaur, Leonardo Seeber and Virendra Tiwari were very helpful. We appreciate comments from the Editor, Duncan Agnew and two anonymous reviewers. ALOS PALSAR data were provided by JAXA through

RA-6, PI NO. 3053. KMS and RA are supported by DMSP R&D program of ISRO.

REFERENCES

Ader, T. et al., 2012. Convergence rate across the Nepal Himalaya and interseismic decoupling on the main Himalayan thrust: implications for seismic hazard, J. geophys. Res., 117, B04403, doi:10.1029/2011JB009071.

Altamimi, Z., Collilieux, X. & Metivier, L., 2011. ITRF2008: an improved solution of the international terrestrial reference frame, J. Geod., doi:10.1007/s00190-011-0444-4.

Bettinelli, P., Avouac, J.P., Flouzat, M., Bollinger, L, Ramillien, G., Rajaure, S. & Sapkota, S., 2008. Seasonal variations of seismicity and geodetic strain in the Himalaya induced by surface hydrology, Earth planet Sci. Lett., 266, 332–344.

Boehm, J., Niell, A., Tregoning, P. & Schuh, H., 2006a. Global Mapping Function (GMF): a new empirical mapping function based on numerical weather model data, Geophys. Res. Lett., 33, L07304, doi:10.1029/2005/GL025546.

Bollinger, L., Perrier, F., Avouac, J.P., Sapkota, S., Gautam, U. & Tiwari, D.R., 2007. Seasonal modulation of seismicity in the Himalaya of Nepal, Geophys. Res. Lett., 34, L08304, doi:10.1029/2006GL029192.

Cavalie, O., Doin, M.-P., Lasserre, C. & Briole, P., 2007. Ground motion mea- ´surement in the Lake Mead area, Nevada, by differential synthetic aperture radar interferometry time series analysis: probing the lithosphere rheological structure, J. geophys. Res., 112, B03403, doi:10.1029/2006JB004344.

Chanard, K., Avouac, J.P., Ramillien, G. & Genrich, J., 2014. Modeling deformation induced by seasonal variations of continental water in the Himalaya region: sensitivity to Earth elastic structure, J. geophys. Res., 119, 5097–5113.

Chen, C.W. & Zebker, H.A., 2001. Two-dimensional phase unwrapping with use of statistical models for cost functions in nonlinear optimization, J. Opt. Soc. Am. A, 18(2), 338–351.

Dill, R., 2008. Hydrological model LSDM for operational Earth rotation and gravity field variations, Scientific Technical Report, 35p., STR08/09, GFZ Potsdam, Germany, doi:10.2312/GFZ.b103-08095.

Dill, R. & Dobslaw, H., 2013. Numerical simulations of global-scale highresolution hydrological crustal deformations, J. geophys. Res., 118, 5008– 5017.

Farrell, W.E., 1972. Deformation of the Earth by surface loads, Rev. Geophys., 10(3), 761–797.

Flouzat, M., Bettinelli, P., Willis, P., Avouac, J.P., Heritier, T. & Gautam, U., 2009. Investigating tropospheric effects and seasonal position variations in GPS and DORIS time-series from the Nepal Himalaya, Geophys. J. Int., 178, 1246–1259.

Fu, Y. & Freymueller, J.T., 2012. Seasonal and long-term vertical deformation in the Nepal Himalaya constrained by GPS and GRACE measurements, J. geophys. Res., 117, B03407, doi:10.1029/2011JB008925.

Fu, Y., Argus, D.F., Freymueller, J.T. & Heflin, M.B., 2013. Horizontal motion in elastic response to seasonal loading of rain water in the Amazon Basin and monsoon water in Southeast Asia observed by GPS and inferred from GRACE, Geophys. Res. Lett., 40, 6048–6053.

Gahalaut, V.K. & Kalpna, 2001. On the geodetic observations during 1965 to 1969 in the Koyna region, J. Geodyn., 31, 499–505.

Gupta, H.K., 1992. Reservoir Induced Earthquakes, Elsevier, 364 pp. Herring, T.A., King, R.W. & McClusky, S.C., 2010a. Documentation of the GAMIT GPS Analysis Software release 10.4, Department of Earth, and Planetary Sciences, Massachusetts Institute of Technology, Cambridge.

Herring, T.A., King, R.W. & McClusky, S.C., 2010b. GLOBK, Global Kalman filter VLBI and GPS analysis program, version 10.4. Department of Earth, and Planetary Sciences, Massachusetts Institute of Technology, Cambridge.

Jaeger, J.C., Cook, N.G.W. & Zimmerman, R.W., 2007. Fundamentals of Rock Mechanics, Blackwell Publishing, 475 pp.

Jonsson, S., Segall, P., Pedersen, R. & Bj ´ ornsson, G., 2003. Post-earthquake ¨ ground movements correlated to pore-pressure transients, Nature, 424, 179–183.

Kaufmann, G. & Amelung, F., 2000. Reservoir-induced deformation and continental rheology in vicinity of Lake Mead, Nevada, J. geophys. Res., 105, 16 341–16 358.

Khandelwal, D.D., Gahalaut, V.K., Kumar, N., Kundu, B. & Yadav, R.K., 2014. Seasonal variation in the deformation rate in NW Himalayan region, Nat. Hazards, doi:10.1007/s11069-014-1269-2.

King, R.W. & Bock, Y., 2005. Documentation of the GAMIT GPS Analysis Software, Massachusetts Institute of Technology.

Lagler, K., Schindelegger, M., Bohm, J., Krasna, H. & Nilsson, T., 2013. ´ GPT2: empirical slant delay model for radio space geodetic techniques, Geophys. Res. Lett. 40, 1069–1073.

Letellier, T., 2004. Etude des ondes de mareesur les plateaux continentaux, ´ Thesedoctorale, Universit ´ e de Toulouse III, 237 pp.

Magilligan, F.J. & Nislow, K.H., 2005. Changes in hydrologic regime by dams, Geomorphology, 71, 61–78.

McCarthy, D.D. & Petit, G. (eds), 2004. IERS conventions (2003), IERS Tech. Note 32, Verl. desBundesamtes fur Kartogr. und Geod., Frankfurt am Main, Germany.

Sandwell, D., Mellors, R., Tong, X., Wei, M. & Wessel, P., 2011. Open radar interferometry software for mapping surface deformation, EOS, Trans. Am. geophys. Un., 92(28), doi:10.1029/2011EO280002.

Simpson, D.W., 1986. Triggered Earthquakes, Annu. Rev. Earth Planet. Sci., 14, 21–42.

van Dam, T.M. & Wahr, J.M., 1987. Displacements of the Earth's surface due to atmospheric loading: effects on gravity and baseline measurements, J. geophys. Res., 92(B2), 1281–1286.

van Dam, T., 2010. Updated October (2010), NCEP Derived 6-hourly, global surface displacements at 2.5 × 2.5 degree spacing, Available at: http://geophy.uni.lu/ncep-loading.html, last accessed 8 March 2016.

Wahr, J., Khan, S.A., van Dam, T., Liu, L., van Angelen, J.H., van den Broeke, M.R. & Meertens, C.M., 2013. The use of GPS horizontals for loading studies, with applications to northern California and southeast Greenland, J. geophys. Res., 118, 1795–1806.

Wang, H., 2000a. Surface vertical displacements and level plane changes in the front reservoir area caused by filling the Three Gorges Reservoir, J. geophys. Res., 105, 13 211–13 220.

Wang, H.F., 2000b, Theory of Linear Poroelasticity with Applications to Geomechanics and Hydrogeology, Princeton Univ. Press, 287 pp.

Wang, T., Perissin, D., Rocca, F. & Ming-Sheng, L., 2011. Three Gorges Dam stability monitoring with time-series InSAR image analysis, Sci. China Earth Sci., 54, 720–732.

Wang, H., Xiang, L., Jia, L., Jiang, L., Wang, Z., Hu, B. & Gao, P., 2012. Load Love numbers and Green's functions for elastic Earth models PREM, iasp91, ak135, and modified models with refined crustal structure from Crust 2.0, Comput. Geosci., 49, 190–199.